PHYSICAL REVIEW B, VOLUME 63, 104404

First-order phase transition in UO_2: ^{235}U and ^{17}O NMR study

K. Ikushima, S. Tsutsui, Y. Haga, H. Yasuoka, and R. E. Walstedt
Advanced Science Research Center, Japan Atomic Energy Research Institute, Tokai, Ibaraki 319-1195, Japan

N. M. Masaki and A. Nakamura
Department of Material Science, Japan Atomic Energy Research Institute, Tokai, Ibaraki 319-1195, Japan

S. Nasu
Department of Material Physics, Faculty of Engineering Science, Osaka University, Toyonaka, Osaka 560-8531, Japan

Y. Ōnuki
Graduate School of Science, Osaka University, Toyonaka, 560-0043, Japan
and Advanced Science Research Center, Japan Atomic Energy Research Institute, Tokai, Ibaraki 319-1195, Japan

(Received 4 October 2000; revised manuscript received 20 November 2000; published 9 February 2001)

A nuclear magnetic resonance (NMR) study is reported for a $5f$-cooperative Jahn-Teller (JT) system with antiferromagnetic ordering, UO_2, where we have performed magnetic actinide (^{235}U) as well as nonmagnetic ligand (^{17}O) NMR studies in a $5f$-electron system. The observed ^{235}U hyperfine interaction is consistent with an axially symmetric $5f$-wave-function character for U^{4+} below a first-order transition temperature $T_N = 30.8$ K. Thus, the orbital degeneracy in the cubic crystalline field is lifted by a magnetic ordering combined with a JT distortion. On the other hand, modulation phenomena in the ^{17}O spin-echo decay provide evidence of a lattice distortion just below T_N, which gives rise to an axially symmetric electric-field gradient at the oxygen sites. These results indicate that, in a cooperative JT transition which occurs as a result of coupling between $5f$ quadrupoles and lattice distortion, the behavior of the $5f$ quadrupoles can be investigated using uranium NMR, while the lattice distortion can be studied with the nonmagnetic ligand NMR. Among magnetic structures and JT distortions, proposed on the basis of neutron scattering experiments and theoretical work, the noncollinear $3\boldsymbol{k}$-type structure is the most likely, because either the $1\boldsymbol{k}$ or $2\boldsymbol{k}$ would cause an orthorhombic distortion. With respect to low-energy spin-wave excitations, nuclear spin-lattice relaxation rates T_1^{-1} at both sites show a T^7 behavior below T_N, which suggests the presence of gapless excitations due to strong magnon-phonon coupling.

DOI: 10.1103/PhysRevB.63.104404 PACS number(s): 75.25.+z, 76.60.−k

I. INTRODUCTION

In magnetic compounds, orbital degeneracy in a highly symmetric crystalline field can become the driving force to generate a phase transition, often with anomalous magnetic behaviors. A well-known example is the so-called cooperative Jahn-Teller (JT) transition in which lattice distortions lift the orbital degeneracy at low temperatures and then an alignment of orbital moments is realized. In the case of *f*-electron systems with strong spin-orbit couplings, we often treat it as the ordering of *f* quadrupoles, which can occur without lattice distortion if an effective quadrupole-quadrupole interaction arises from exchange-type interactions through conduction electrons.

Recently, studies with respect to quadrupole degrees of freedom have been carried out not only for well-localized $4f$-electron systems but also for uranium intermetallic compounds in which the $5f$ electrons can show more itinerant character. This may be a key point for understanding anomalous magnetic states as typified by the antiferromagnetic (AFM) ordering with a tiny moment, $\sim 0.02\mu_B$, observed in UPd_3 (Ref. 1) and URu_2Si_2 (Ref. 2). In order to discuss these exotic microscopic properties found in uranium intermetallic compounds, we need to know the typical local properties of U^{4+} ($5f^2$) or U^{3+} ($5f^3$) ions under the crystalline field in more detail. As the first step, we have performed ^{235}U and ^{17}O NMR studies in uranium dioxide, UO_2, which one can regard as a well-localized $5f^2$-electron system.

Uranium dioxide is an ionically bounded semiconductor with U^{4+} ions ($^3H_4$). The crystal structure of UO_2 is the face-centered-cubic fluorite structure. In the presence of a cubic crystalline field, the ninefold degeneracy of the $^3H_4$ state is reduced to triplet Γ_5 and Γ_4 states, a doublet Γ_3, and a singlet Γ_1. Rahman and Runciman predicted the Γ_5 ground triplet separated by 170 meV from a first excited Γ_3 doublet, diagonalizing the complete Hamiltonian for UO_2 including Coulomb, spin-orbit, and crystal-field terms.[3] In fact, pulsed neutron experiments observe such an excitation at 150 meV.[4] The degeneracy of a ground state with an even number of electrons per magnetic ion can be lifted by magnetic or quadrupolar ordering at low temperatures. Of this, uranium dioxide is a striking example with a single first-order magnetic transition, suggesting that the exchange interactions and the quadrupole-quadrupole interactions via phonons are comparable in size.[8]

From the Curie-Weiss behavior of the magnetic susceptibility, the effective moment is estimated to be about $3.0\mu_B$, which is somewhat larger than that of the Γ_5 ground state, $2.83\mu_B$, but smaller than that of the $^3H_4$ state, $3.58\mu_B$. Uranium dioxide shows a type-I AFM structure with (001)

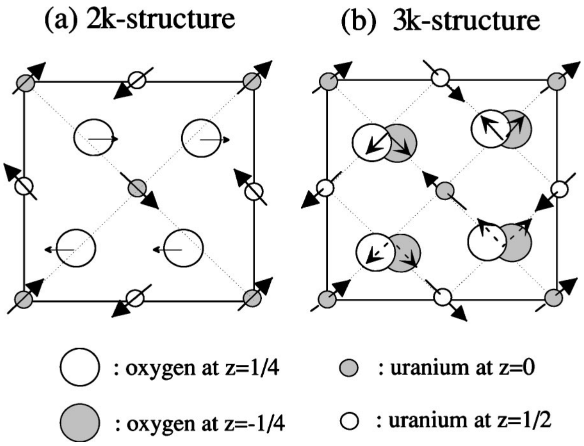

FIG. 1. The (001) projection of the fluorite structure to display the $2\boldsymbol{k}$ and $3\boldsymbol{k}$ structures which are possible in UO_2 (Ref. 10). In the $2\boldsymbol{k}$ structure the displacements are along $\langle 010\rangle$, whereas in the $3\boldsymbol{k}$ structure they occur along $\langle 111\rangle$; dashed and solid arrows are for down and up displacements. In a $2\boldsymbol{k}$ structure the magnetic moments lie along $\langle 110\rangle$ whereas in a $3\boldsymbol{k}$ structure they are along $\langle 111\rangle$.

ferromagnetic planes[5] below $T_N = 30.8 \pm 0.3$ K. In a multidomain crystal, the directions of moments cannot be determined by neutron diffraction. However, as a result of a detailed analysis, Faber and Lander proposed a noncollinear $2\boldsymbol{k}$ structure where moments occupy all four $\langle 110\rangle$ directions within an (001) plane [Fig. 1(a)].[6] They also found a small shift (0.014 Å) of the oxygen atoms from their equilibrium position with no change in the unit cell dimensions. The magnetic excitations in the AFM state were measured by Cowley and Dolling, who identified the first example of an interaction between magnons and phonons.[7] Recent inelastic neutron scattering experiments have confirmed the results obtained by Cowley and Dolling, and furthermore observed a dispersive inelastic response between 3 and 10 meV even in the paramagnetic state above T_N, suggesting the presence of a $1\boldsymbol{k}$ rather than multi-$\boldsymbol{k}$ dynamical JT distortions.[9]

The theory of UO_2 by Allen gives a satisfactory explanation of the first-order phase transition through the spin-lattice interaction.[8] The physical mechanism for the quadrupolar coupling is a modification of the crystalline field acting on the $5f$ electrons by the motion of surrounding O^{2-} ions. Allen's model, however, assumed a $1\boldsymbol{k}$ structure, whereas in the model of Faber and Lander the $2\boldsymbol{k}$ structure in Fig. 1(a) was proposed. Furthermore, as a result of more careful analysis[10,11] or neutron scattering experiments under a magnetic field,[12] the $3\boldsymbol{k}$ structure with the $3\boldsymbol{k}$ crystallographic distortion was also proposed as seen in Fig. 1(b). On the other hand, experimental NMR studies of actinide sites have never been reported in solids, because the ^{235}U nucleus has the extraordinarily small nuclear gyromagnetic ratio of 0.784 MHz/T and a poor natural abundance of 0.72%. It is therefore very difficult to detect ^{235}U NMR signals in a sample prepared using natural uranium under an applied magnetic field of about 10 T. In addition, the actinide nuclear relaxation times T_1 and T_2 are usually too short in magnetic compounds because of the extremely large orbital hyperfine field and the small characteristic energy scale. Recently, we have observed ^{171}Yb NMR signals in the Kondo semiconductor YbB_{12},[13] but only at temperatures much lower than the energy gap. So we have performed the ^{235}U NMR at $T \ll T_N$, since we can expect a moderately long relaxation time due to the spin-wave gap in the AFM state. In this study, we have performed zero-field NMR experiments to utilize the large hyperfine field from the U^{4+} ions in a magnetically ordered state. Further, we have prepared 93% ^{235}U-enriched samples. As a result, we succeeded in observing ^{235}U NMR signals at zero applied field, of which papers have already been published in Refs. 14 and 15. In Sec. IV A, we discuss the ^{235}U hyperfine interaction in more detail. Another important result is the observation of an axially symmetric electric-field gradient (EFG) at oxygen sites below T_N via ^{17}O spin-echo modulation caused by the quadrupole splitting. This leads to the conclusion that the $3\boldsymbol{k}$ structure is the most likely of magnetic structures proposed on the basis of the neutron scattering experiments.

II. EXPERIMENTAL PROCEDURE

We prepared two 93% ^{235}U-enriched samples of UO_2. One (UO_2 No. 1) was made by heating uranium oxide at 1273 K under an atmosphere of hydrogen. Another sample (UO_2 No. 2) was made by oxidizing ^{235}U-metal powder which had been pulverized into small particles by heating a purified ^{235}U-metal ingot at 673 K under an atmosphere of hydrogen. The x-ray diffraction patterns of both samples were well indexed by the cubic fluorite structure with a lattice constant of $a = 5.47$ Å, but the peak near the phase transition (30.5 K) in the magnetic susceptibility of UO_2 No. 2 is clearer than that of UO_2 No. 1, and the Curie term of UO_2 No. 2 at low temperatures, which could be attributed to local moments of impurities, is almost unobservable. Both samples were pressed into 7-mm-diam pellets and sintered under an atmosphere of hydrogen, because of the better filling factor resulting in a better S/N ratio for NMR signals and shorter pulses for the available power. An ^{17}O enriched sample of UO_2 was prepared by a similar method to that of UO_2 No. 2. This powdered sample was sealed in a quartz tube of diameter 8 mm.

The NMR experiments were carried out using a conventional pulsed phase-coherent spectrometer. In NMR measurements at zero field, a pulsed, phase-incoherent spectrometer was also used to simplify experimental conditions. The high-speed averaging function of a digital storage scope was utilized for measurements of nuclear spin-lattice relaxation rates. The ^{17}O (nuclear spin $I = 5/2$) NMR spectra, obtained by sweeping a magnetic field at a constant frequency ν_0, were measured by recording the output of a boxcar integrator. Magnetic fields were applied using a superconducting solenoid with a maximum field of 12 T. We obtained the NMR shift K from the following relation:

$$K = \frac{H_0 - H_{\mathrm{res}}}{H_{\mathrm{res}}} \times 100\%, \tag{1}$$

where $H_0 = \nu_0/\gamma_N$, and H_{res} is the field evaluated from the peak position of the spectrum. For the ^{17}O NMR, $^{17}\gamma_N = 5.772$ MHz/T and $\nu_0 = 62.1$ MHz.

The search for ^{235}U ($I = 7/2$) resonance signals was performed using UO_2 No. 1 sample at zero field and below 4.2 K. Since the hyperfine field at the U sites is estimated as 270 ± 20 T from the Mössbauer experiments,[16,17] we concentrated our search on frequencies between 150 and 250 MHz. The ^{235}U NMR spectrum was obtained by measuring the intensities of spin-echo signals averaged by the digital storage scope at each frequency.

The nuclear spin-lattice relaxation rate T_1^{-1} was measured by the standard saturation recovery technique. A single saturation pulse is applied at time t before a spin-echo sequence, and the recovery of nuclear magnetization is obtained by changing t. The nuclear spin-lattice relaxation rate is determined by fitting recovery curves, for ^{17}O NMR in the absence of quadrupole splitting, to a single exponential function,

$$\frac{M(\infty)-M(t)}{M(\infty)} = M_0 \exp\left(-\frac{t}{T_1}\right), \tag{2}$$

and for ^{235}U NMR, to the following function for the magnetic relaxation process:

$$\frac{M(\infty)-M(t)}{M(\infty)} = M_0\left[A \exp\left(-\frac{t}{T_1}\right) + B \exp\left(-\frac{6t}{T_1}\right) + C \exp\left(-\frac{15t}{T_1}\right) + D \exp\left(-\frac{28t}{T_1}\right)\right]. \tag{3}$$

Here $M(t)$ and $M(\infty)$ are the nuclear magnetization at time t after the saturation pulse and at thermal equilibrium, respectively. In Eq. (3), A, B, C, D, and M_0 are equal to 1/84, 3/44, 75/364, 1225/1716, and 1, respectively, if the initial condition is such that the central transition ($I = 1/2 \leftrightarrow -1/2$) is completely saturated and populations of the other spin levels are unaffected. The recovery curve could be fitted more accurately for the UO_2 No. 2 sample than the UO_2 No. 1 sample, although no substantial difference of spectra was observed between these samples. The recovery curve in the UO_2 No. 1 sample might be affected by a relaxation process due to the local magnetic impurities which show a Curie term at low temperatures in the magnetic suceptibility.

III. EXPERIMENTAL RESULTS

A. ^{235}U NMR

Seven ^{235}U ($I = 7/2$) resonance lines have been observed in UO_2 at 1.5 K and zero field.[13] The ^{235}U spin-echo spectrum is shown in Fig. 2. As far as we know, this is the first NMR observation for magnetic actinide ions. The hyperfine field at the U sites is evaluated as 252.3 ± 0.5 T, which agrees with that obtained from the ^{238}U Mössbauer experiments within their experimental errors.[16,17] The extremely large hyperfine field is considered to be the orbital field due to $5f$ electrons of the $^3H_4$ state. The most striking feature is that the electric quadrupole interaction at the ^{235}U sites is clearly observed, although it was not observed in the ^{238}U Mössbauer spectrum because of the inherently poor resolution. In rare earth and actinide ions an electric quadrupole interaction normally exists even at a site of cubic symmetry if magnetic ordering is present, because the spatial alignment of the magnetic moments also implies that of the orbital angular momentum, resulting in an axially symmetric charge distribution around the nucleus. Almost equal separation of the resonance frequencies, 14 ± 0.4 MHz, indicates an axially symmetric EFG at the ^{235}U sites. Thus, we obtain the electric quadrupole interaction as follows:

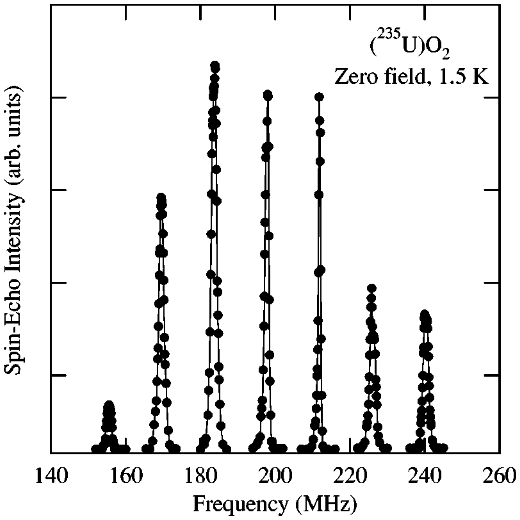

FIG. 2. ^{235}U spin-echo spectrum in the AFM state of UO_2 at 1.5 K.

$$\left|\frac{e^2qQ}{h}(3\cos^2\theta - 1)\right| = 392 \pm 11 \text{ MHz}, \tag{4}$$

where eq is the maximum principal component of the EFG tensor evaluated at the nucleus, Q is the nuclear quadrupole moment, and θ is the angle between the principal axis of the maximum EFG tensor and the direction of the hyperfine field. The analyses of the magnetic hyperfine field and the electric quadrupole interaction produced by f electrons will be performed in Sec. IV A, showing that the observed quadrupole interaction is of the same order as the hyperfine splitting produced by the Γ_5 ground state of U^{4+}.

We have measured the T dependence of the magnetic hyperfine field H_{hf} and the quadrupole splitting in the AFM state of UO_2. The signals cannot be observed above 14 K because of too short relaxation time. Below 14 K there is little variation in the magnetic hyperfine field or the quadrupole splitting. This indicates no change in the distribution of $5f$ electrons around the nucleus at low temperatures, and is consistent with a similar finding by neutron scattering for the ordered moment.

Figure 3 shows the T dependence of the ^{235}U nuclear spin-lattice relaxation rate $^{235}(T_1^{-1})$, which exhibits T^7-like rather than activated behavior. The spin wave excitations in UO_2 will be discussed in Sec. IV C.

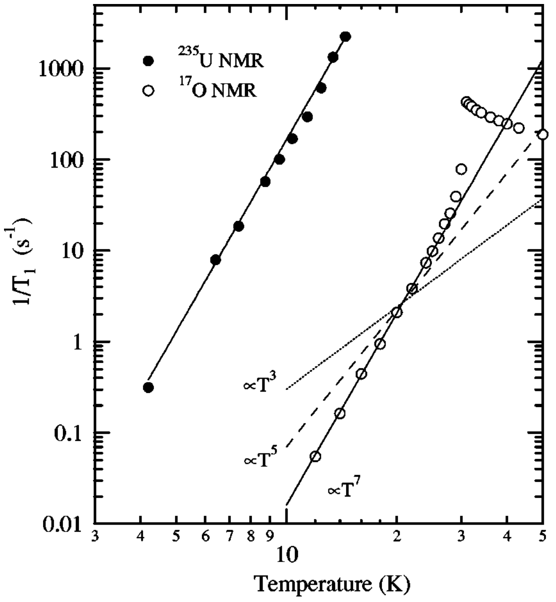

FIG. 3. Temperature dependence of $(1/T_1)$ in the AFM state. The solid and open circles represent the relaxation rates for ^{w35}U and ^{17}O nuclei, respectively.

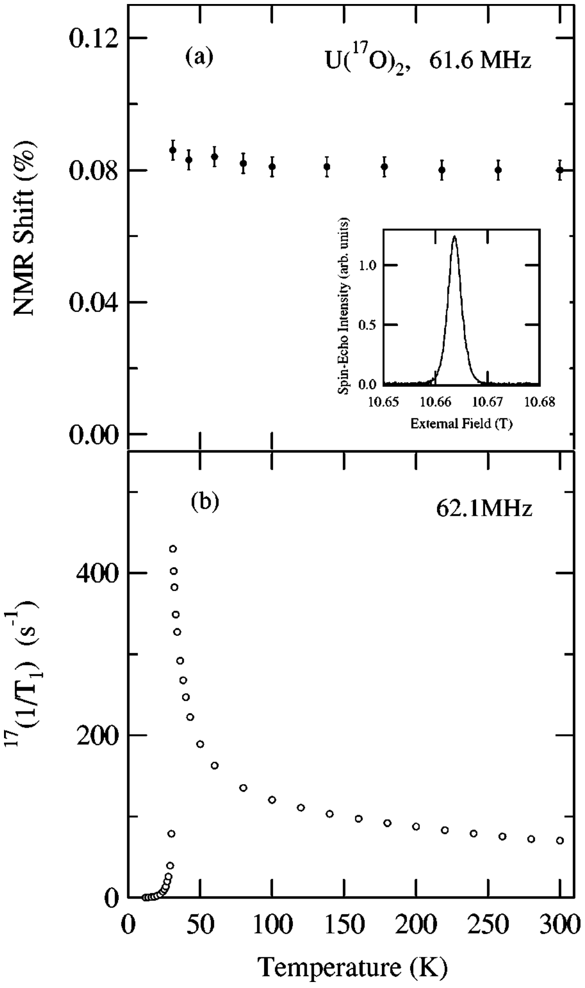

FIG. 4. (a) Temperature dependence of the NMR shift at the ^{17}O sites at 61.6 MHz in the paramagnetic state, which indicates a rather small transferred hyperfine coupling constant. The inset shows the ^{17}O spin-echo spectrum in the paramagnetic state. It is measured with the pulse condition of 4.2 μs–τ–8.4 μs. (b) Temperature dependence of $^{17}(1/T_1)$ at 62.1 MHz, which stands in sharp contrast with the constancy of the ^{17}O NMR shifts in the paramagnetic state.

B. ^{17}O NMR

The ^{17}O$(I=5/2)$ NMR spectrum in the paramagnetic state, obtained from spin-echo signals with a pulse condition of 4.2 μs–τ–8.4 μs at 300 K and 61.6 MHz, is shown in the inset of Fig. 4(a). The symmetric spectrum with a full width at half maximum (FWHM) of 3×10^{-3} T indicates no quadrupole splitting and no anisotropy of the NMR shift, which can be understood from the cubic point symmetry at the ^{17}O sites. Figure 4(a) presents the T dependence of the NMR shift. The weak T dependence of the NMR shift suggests that the transferred hyperfine field is rather small. In the K vs χ analysis, the isotropic hyperfine coupling constant $^{17}A_{\rm iso}$ is estimated to be about 10^{-3} T/$\mu_{\rm B}$. This means that overlap with the $5f$ wave functions is of secondary importance. On the other hand, in the paramagnetic state, the nuclear spin-lattice relaxation rate T_1^{-1} rapidly increases as T decreases towards $T_{\rm N}$ as seen in Fig. 4(b). This behavior stands in marked contrast with the T-independent NMR shift, which reflects local uniform susceptibility $\chi(q=0,\omega=0)$ at the oxygen sites. Using the Fourier components A_q of the transverse hyperfine coupling constant and the imaginary part of the transverse dynamical susceptibility $\chi''(q,\omega)$, we can generally express the nuclear spin-lattice relaxation rate as[18]

$$\frac{1}{T_1}=\frac{2k_{\rm B}T\gamma_{\rm N}^2}{\mu_{\rm B}^2}\sum_q |A_q|^2\chi''(q,\omega_{\rm N}), \tag{5}$$

where $k_{\rm B}$ and $\omega_{\rm N}$ are Boltzmann's constant and the NMR frequency, respectively. Assuming that the hyperfine field at the oxygen sites is dominated by an isotropic transferred hyperfine field from f moments at the uranium sites rather than an on-site hyperfine field, the Fourier component $|^{17}A_q|^2$ can be calculated to be

$$|^{17}A_q|^2=|^{17}A_{q=0}|^2|^{17}f(q)|^2, \tag{6}$$

where

$$|^{17}A_{q=0}|=|^{17}A_{\rm iso}|\sim10^{-3}\ {\rm T}/\mu_{\rm B},$$

$$|^{17}f(q)|^2=\cos^2(q_xa/2)\cos^2(q_ya/2)\cos^2(q_za/2)$$
$$+\sin^2(q_xa/4)\sin^2(q_ya/4)\sin^2(q_za/4). \tag{7}$$

In Eq. (6), the $f(q)$ is the hyperfine form factor. The important point is that the form factor at the oxygen sites is canceled just at an AFM wave vector $\boldsymbol{Q}=(2\pi/a)(0,0,1)$. In the same way, we confirm that the form factor due to dipolar field is also zero just at $\boldsymbol{Q}$. According to the inelastic neutron scattering experiments, a large quasielastic response having a Lorentzian shape with spatial correlation length $\xi=5.5$ Å at 31.7 K is observed above $T_{\rm N}$ around $\boldsymbol{Q}$.[9,19] Although these form factors are canceled out just at $\boldsymbol{Q}$, the $^{17}(T_1^{-1})$ should reflect the enhanced AFM components around $\boldsymbol{Q}$ within a

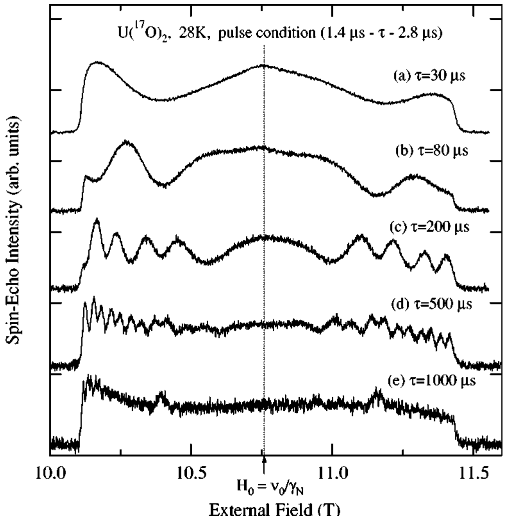

FIG. 5. ^{17}O spin-echo spectrum in the AFM state of UO$_2$ at 62.1 MHz for various time intervals between $\pi/2$ and π pulses. The dotted line represents the position of $H_0 = \nu_0/\gamma_N$. The spectrum (e) corresponds to the typical powder pattern spectrum in the AFM state.

range of $1/\xi$ rather than $q=0$ in the dynamical susceptibility. Considering that the dipolar field at the oxygen sites is two orders of magnitude larger than the observed isotropic hyperfine field, the relaxation process via the dipolar field would be dominant in $^{17}(T_1^{-1})$. Another possible interpretation for the behavior of $^{17}(T_1^{-1})$ in the paramagnetic state is that the $^{17}(T_1^{-1})$ probes the character of the dynamical JT distortion above T_N in a relaxation process due to EFG fluctuations (quadrupole relaxation) rather than magnetic hyperfine fluctuations (magnetic relaxation). Quadrupole relaxation at the ^{17}O sites, however, is usually not expected below the Debye temperature, $\sim$200 K, because of the small ^{17}O nuclear quadrupole moment of 2.6×10^{-2} barns.

We also report interesting ^{17}O NMR results for the AFM state. Spin-echo spectra broaden drastically below T_N and depend strongly on the pulse conditions for echo formation, ''first pulse–τ–second pulse,'' where τ is the separation between excitation rf pulses. In Fig. 5, spin-echo spectra under the conditions 1.4 μs–τ–2.8 μs are shown for several time intervals τ at 28 K. As seen in Fig. 6, the anomalous τ dependence of the spin-echo spectra is attributable to a modulation in the spin-echo decay, for which the period depends surprisingly on the resonance field. Thus, we cannot measure an intrinsic spin-echo spectrum by sweeping the magnetic field unless τ is long enough so that the modulation effect is negligible. In fact, the spectrum at $\tau=1000$ μs is similar to a typical powder pattern spectrum in the AFM state for the sites for which the internal field $H_{\rm int}$ is smaller than the applied external field $H_{\rm ext}$. In the powder pattern spectrum, spin-echo signals at the extrema arise from sites with internal fields antiparallel and parallel to the external field, respectively. As a result, the linewidth corresponds to $2H_{\rm int}$ and in the case of $H_{\rm ext} \gg H_{\rm int}$ the spectrum will be nearly symmetric with respect to a resonance field, $H_0 = \nu_0/\gamma_N$. From the linewidth in Fig. 5(e), the internal field at the oxygen sites is roughly estimated to be about 0.65 T. Furthermore, an unexpected spectrum is also obtained with the same pulse condition, 4.2 μs–τ–8.4 μs, as was used for the paramagnetic state [Fig. 7(b)]. Two resonance peaks, al-

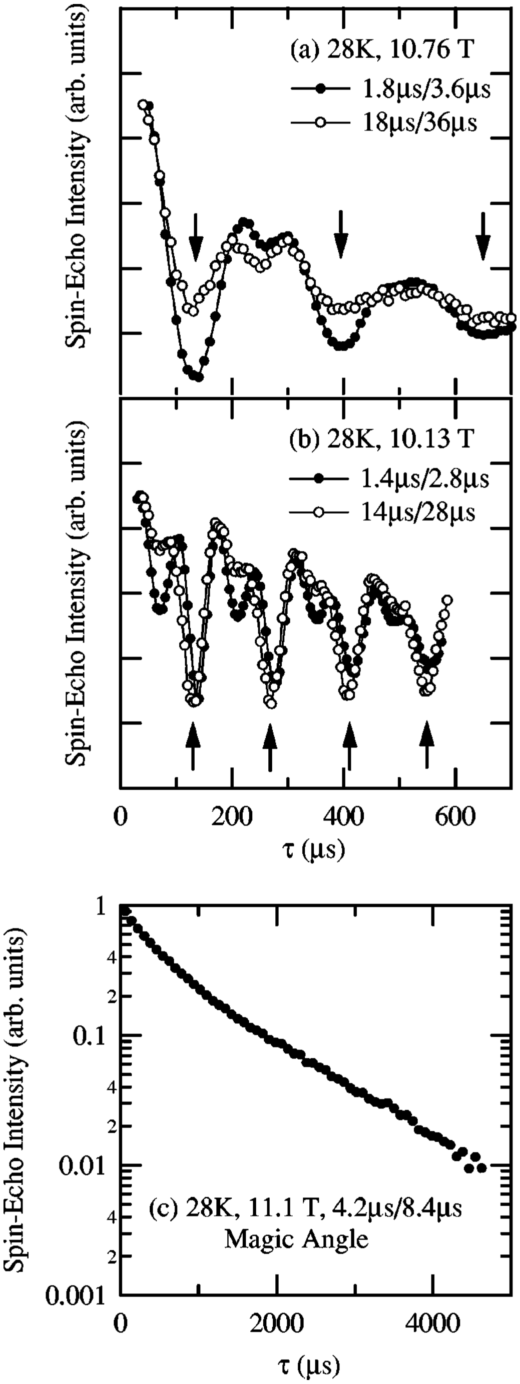

FIG. 6. ^{17}O spin-echo decay curves: (a) at an edge on the lower field side in the spectrum of Fig. 5(e), (b) at the resonance field $H_0 = \nu_0/\gamma_N$, and (c) at the peak in Fig. 7(b). The arrows in (a) and (b) represent minima of spin-echo oscillations corresponding to the quadrupole splitting. Second-harmonic terms with half of that period are also observed, even on the pulse condition of 14 μs–τ–28 μs or 18 μs–τ–36 μs. The asymmetric feature of the modulation strongly depends on the pulse condition, but the period is not affected.

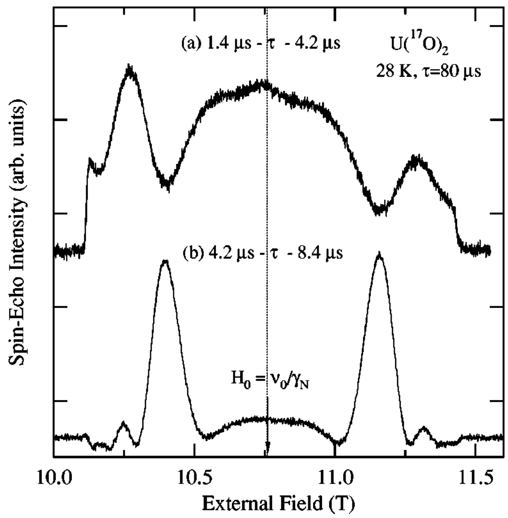

FIG. 7. ^{17}O spin-echo spectra with different pulse conditions. The spectrum (b) is measured with the same pulse condition as 4.2 μs–τ–8.4 μs used in the paramagnetic state.

most symmetrically split with respect to H_0, are observed at $H_{\rm ma}^{\pm}$.

These somewhat surprising NMR results can be understood in terms of an axially symmetric EFG at the ^{17}O sites in the AFM state as follows. The first-order quadrupole splitting $a(\theta)$ can cause spin-echo modulation with a period, $2\pi/a$. In general, we can express the spin-echo amplitude $E(2\tau)$ for $I=5/2$ as[20]

$$\begin{aligned}E(2\tau)=&c_0+c_1\cos[a(\theta)\tau+\delta_1]+c_2\cos[2a(\theta)\tau+\delta_2]\\&+c_3\cos[3a(\theta)\tau+\delta_3]+c_4\cos[4a(\theta)\tau+\delta_4],\end{aligned}\tag{8}$$

where

$$\begin{aligned}\frac{a(\theta)}{2\pi}&=|(3e^2qQ)(3\cos^2\theta-1)/[4hI(2I-1)]|\\&=\left|\frac{\nu_Q}{2}(3\cos^2\theta-1)\right|.\end{aligned}\tag{9}$$

The coefficients c_j and δ_j are quite sensitive to excitation pulse conditions. θ is the angle between $\boldsymbol{H}_{\rm ext}$ and the principal axis of the EFG tensor (Z axis). ν_Q is the electric quadrupole frequency parameter. As seen in Fig. 6, modulation periods at the edges of the spin-echo spectrum are just half of that at H_0; that is, the splittings $a(\theta)$ at the edges are just twice as large as that at H_0. This means that the angle θ is 0 and $\pi/2$ at the edges and at H_0, respectively. Since $H_{\rm int}$ is parallel and perpendicular to $H_{\rm ext}$ at the edges and at H_0, respectively, we conclude that the internal field at the oxygen sites is parallel to the Z axis. In Figs. 6(a) and 6(b), higher-harmonic terms with period π/a are also observed, attributed to an excitation condition where the rf pulses excite multiple quadrupolar satellites as well as the central line.[20] In this case, the oscillatory behavior of the spin-echo decay curve depends strongly on the pulse conditions, but the period is not affected. In fact, we confirm the constancy of the period by measuring the spin-echo decay with different pulse conditions as seen in Figs. 6(a) and 6(b). Furthermore, no spin-echo modulation is observed for the two resonance peaks at $H_{\rm ma}^{\pm}$ [Fig. 6(c)]. This indicates that signals at $H_{\rm ma}^{\pm}$ are observed at the ‘‘magic angle’’ condition with $\theta=\cos^{-1}(1/\sqrt{3})\equiv\alpha$ in which the first-order quadrupole splitting vanishes. This magic angle condition is also supported by the result that separation between $H_{\rm ma}^{\pm}$ and H_0 is just $1/\sqrt{3}$ times half width of the spectrum in Fig. 5(e). The reason why the characteristic spectrum with two peaks is observed only near a pulse condition of 4.2 μs–τ–8.4 μs can be also explained by the presence of the quadrupole splitting. The effective rf field for the central transition ($1/2\leftrightarrow-1/2$) split by the nuclear electric quadrupole interaction is 3 times as large as that for the NMR line in the absence of a quadrupole splitting.[21] Since the $\pi/2$ pulse width tipping the magnetization is inversely proportional to the amplitude of rf field, the $\pi/2$ pulse width for the central transition alone is 1/3 of that for the NMR line in the absence of a quadrupole splitting. Such a characteristic spectrum is therefore obtained only near the same pulse condition, 4.2 μs–τ–8.4 μs, as used in the paramagnetic state without a quadrupole splitting.

To study the NMR shift and the internal field below $T_{\rm N}$, we can express $H_{\rm ma}^{\pm}$ as follows:

$$H_{\rm ma}^{\pm}=\frac{H_0\pm H_{\rm int}\cos\alpha}{1+K_\alpha}=\frac{H_0\pm\frac{1}{\sqrt{3}}H_{\rm int}}{1+K_\alpha},\tag{10}$$

where $K_\alpha=[H_0\pm(1/\sqrt{3})H_{\rm int}-H_{\rm ma}^{\pm}]/H_{\rm ma}^{\pm}$ is defined as the NMR shift at the angle α. This can also be rewritten as

$$K_\alpha=H_0/[(H_{\rm ma}^{-}+H_{\rm ma}^{+})/2]-1,\tag{11}$$

which represents the shift of the central field from H_0. Using $H_{\rm ma}^{\pm}$, we have determined the K_α over a range of temperatures $T<T_{\rm N}$. The T dependence of K_α is shown in the inset of Fig. 8. The K_α evidently represents a background chemical shift which appears when the transferred hyperfine couplings from the uranium sites are removed. From the value of K_α and $H_{\rm ma}^{\pm}$, we obtain the T dependence of the internal field from Eq. (10) (Fig. 8).

On the assumption of an axially symmetric EFG tensor and $H_{\rm int}\|Z$ axis at the ^{17}O sites, the angle θ can be written by

$$\cos\theta=(H_0-H_{\rm res})/H_{\rm int},\tag{12}$$

where $H_{\rm res}$ is the external field at which the resonance is observed. The solid curve in Fig. 9 represents the result calculated by substituting $H_{\rm int}=0.659$ T and $\nu_Q=7.6$ kHz at 28 K into Eqs. (9) and (12). The presence of an axially symmetric EFG at the oxygen sites is confirmed by the good agreement with the measured frequencies in Fig. 9. Here, ν_Q is evaluated as twice the modulation frequency at $H_{\rm res}=H_0$. We also measured the T dependence of ν_Q, which shows a dramatic onset just below $T_{\rm N}$ (Fig. 8). In Sec. IV B, we will discuss the magnetic structure and the Jahn-Teller distortion of UO$_2$ on the basis of these results.

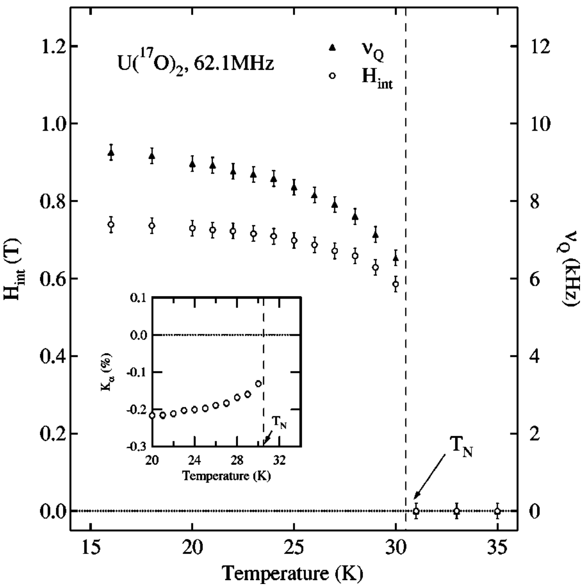

FIG. 8. Temperature dependence of the internal field and the nuclear quadrupole frequency at the ^{17}O sites in the AFM state. The inset shows the temperature dependence of K_α.

In the AFM state, $^{17}(1/T_1)$ has been measured for the peaks at $H_{\rm ma}^{\pm}$ in Fig. 7(b). In this case, we can fit nuclear magnetization recovery curves to a single-exponential function [Eq. (2)] because of the absence of quadrupole splittings at the magic angle condition. The T dependence of $^{17}(1/T_1)$ is shown in Fig. 3. It drops rapidly below $T_{\rm N}$, showing a T^7-like behavior at low temperatures similar to the result for the ^{235}U NMR.

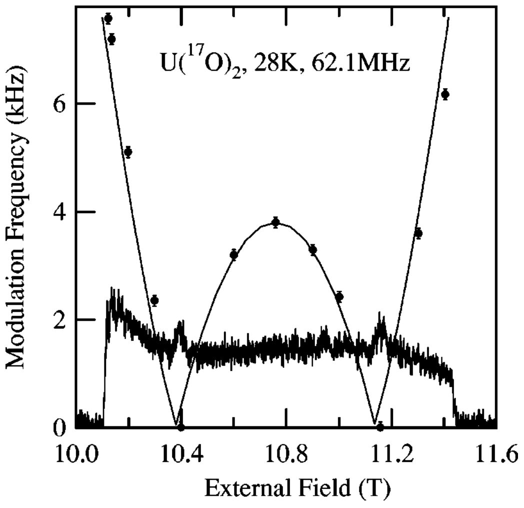

FIG. 9. Field dependence of the modulation frequency in the spin-echo decay (solid circles). The solid curve is calculated with $H_{\rm int}=0.659$ T and $\nu_Q=7.6$ kHz on the assumption that the modulation is caused by the quadrupole splitting due to the axially symmetric EFG.

IV. DISCUSSION

A. Hyperfine interaction on U^{4+} ions

In $5f^2$ with LS coupling one has $J=L-S$ with $L=5$, $S=1$ for ^{3}H$_4$ ground term. Within this manifold, the magnetic hyperfine interaction can be written as $A_J(\boldsymbol{J}\cdot\boldsymbol{I})$ with[22]

$$A_J=\frac{2\mu_{\rm B}\gamma_{\rm N}\hbar}{J(J+1)}[\langle r_l^{-3}\rangle(\boldsymbol{L}\cdot\boldsymbol{J})+\langle r_s^{-3}\rangle(\boldsymbol{S}\cdot\boldsymbol{J})+\langle r_{sC}^{-3}\rangle\xi\{L(L+1)(\boldsymbol{S}\cdot\boldsymbol{J})-3(\boldsymbol{L}\cdot\boldsymbol{J})(\boldsymbol{L}\cdot\boldsymbol{S})\}], \quad (13)$$

and then using Landé factor g_J we can write the orbital (H_J^{orb}), spin (H_J^{spin}) and (H_J^{sC}) contributions to the hyperfine fields as follows:[22]

$$H_J^{orb}=2\mu_{\rm B}\langle r_l^{-3}\rangle(2-g_J), \quad (14)$$

$$H_J^{spin}=2\mu_{\rm B}\langle r_s^{-3}\rangle(g_J-1), \quad (15)$$

$$H_J^{sC}=2\mu_{\rm B}\langle r_{sC}^{-3}\rangle\xi\{L(L+1)(g_J-1)-3(2-g_J)(\boldsymbol{L}\cdot\boldsymbol{S})\}. \quad (16)$$

Here, $\langle r_l^{-3}\rangle$, $\langle r_s^{-3}\rangle$, and $\langle r_{sC}^{-3}\rangle$ are spatial averages for the orbital, spin, and spin-dipole hyperfine interactions, respectively, and ξ, a factor determined by the $(\boldsymbol{L},\boldsymbol{S})$ term, is 1/135 for a U^{4+} ion. Assuming $\langle r_l^{-3}\rangle=\langle r_{sC}^{-3}\rangle=\langle r^{-3}\rangle$ and $\langle r_s^{-3}\rangle=0$ in the nonrelativistic theory, the hyperfine coupling constant A_J is given by $2\mu_{\rm B}\gamma_{\rm N}\hbar\langle r^{-3}\rangle\langle J\|N\|J\rangle$ where $\langle J\|N\|J\rangle$ is a factor which is independent of the magnetic quantum number within the J manifold.

Using the measured hyperfine field, 253.2±0.5 T, and the ordered magnetic moment, $1.74\pm0.02\ \mu_{\rm B}$,[6] we obtain $A_{\rm hf}/g_J=145\pm2$ T/$\mu_{\rm B}$ where $J=4$ and $g_J=4/5$. For actinide series, a relativistic correction of $\langle r^{-3}\rangle$ is calculated by using a relativistic equivalent of the Slater-modified Hartree-Fock method.[23] We thus calculated the hyperfine coupling constants A_J/g_J for a free U^{4+} ion on the basis of the nonrelativistic and relativistic theories. These results are summarized in Table I. We find that the nonrelativistic calculation gives comparable results with the values of $\langle r^{-3}\rangle$ including relativistic corrections but somewhat causes an overestimation of the hyperfine coupling constant. For the core-polarization field, no theoretical calculation has been performed for actinide ions. Dunlap and Kalvius, however, have evaluated core-polarization fields from Mössbauer experiments for some actinide ions, and concluded that this is more substantial for actinides than rare earth series.[25,26] Assuming that the total density of unpaired s spins induced by $5f$ spin polarization is constant per $5f$ electron for the entire actinide series as in the case of transition metals, we can roughly estimate a value of $H_{\rm core}$ for uranium ions as shown in Table I. An important point is that core-polarization fields for actinide ions are positive unlike in the $3d$ or $4d$ transition metals. It is therefore possible that the difference between the experimental value and the calculated A_J/g_J term is attributed to core-polarization fields.

On the other hand, the nuclear quadrupole interaction produced by surrounding electrons depends strongly on the elec-

TABLE I. Hyperfine coupling constants of a free uranium ion. In the nonrelativistic (NREL) estimation, we use $\langle r^{-3}\rangle = 7.82$ a.u. for a free U^{4+} ion.[24] In the relativistic (REL) estimation, each contribution of the hyperfine field is calculated from Eq. (13) by using $\langle r_l^{-3}\rangle = 6.164$ a.u., $\langle r_{sC}^{-3}\rangle = 7.105$ a.u., or $\langle r_s^{-3}\rangle = -0.431$ a.u. The values of H_{core} are estimated from the experimental results of Pu^0, Pu^{3+}, Am^0, and Am^{2+} Mössbauer measurements (Refs. 25 and 26), assuming that the total density of unpaired *s* spins induced by $5f$ spin polarization is constant per $5f$ electron for the entire actinide series.

	H_J^{orb} (T)	H_J^{sC} (T)	H_J^{s} (T)	H_J (T)	A_J/g_J (T/μ_B)	H_{core} (T)	A_{hf}/g_J (T/μ_B)
NREL calculation							
U^{4+}	472	44	–	516	161	~48	~176
REL calculation							
U^{4+}	370.4	41.2	4	415.6	129.9	~48	~145
Experiment (U^{4+})	–	–	–	–	–	–	145±2 (UO_2)

tronic state in the crystalline field. In general, the principal component of the EFG is a sum of several contributions. For UO_2, we can write

$$eq = eq_{5f}(1-R_{5f}) + eq_{\mathrm{lattice}}(1-\gamma_\infty) + eq'. \qquad (17)$$

The first term on the right-hand side of Eq. (17) represents the contribution to the EFG produced by $5f$ electrons and R_{5f} is the Sternheimer factor[27] which describes the modification of the EFG by the inner electrons. The second term represents the contribution from charged sites and γ_∞ is the corresponding Sternheimer factor. The last term gives an EFG from bonding orbitals if the $5f$ electrons participate in bonding. The small transferred hyperfine field at the oxygen sites indicates that participation in bonding by the $5f$ electrons is minor. Thus, in the discussion below, we neglect the last term in Eq. (17).

The principal EFG component eq_{5f} produced by $5f$ electrons for a free ion is given by[22]

$$eq_{5f} = -e\alpha_J\langle r_q^{-3}\rangle\langle\psi|3J_z^2 - J(J+1)|\psi\rangle, \qquad (18)$$

where α_J is a reduced matrix element tabulated by Elliott and Stevens,[28] $\langle r_q^{-3}\rangle$ is an effective radial parameter for the nuclear electric quadrupole interaction, and $\langle\psi|V|\psi\rangle$ represents the diagonal matrix element of operator V for the Hund state $|\psi\rangle$. Equation (18) means that we can get the expectation value of the $5f$ quadrupole tensor $O_2^0 = 3J_z^2 - J(J+1)$ by measuring the ^{235}U nuclear quadrupole splitting. Also for the EFG produced by $5f$ electrons under a crystalline field, we can obtain a formula similar to Eq. (18). In the case of the Γ_5 triplet for $J=4$, eq_{5f} is given by the following formula with fictious spin $\tilde{S}=1$:[22]

$$eq = -e\alpha_J\langle r_q^{-3}\rangle\langle\tilde{1}|3\tilde{S}_z^2 - \tilde{S}(\tilde{S}+1)|\tilde{1}\rangle \times\langle\tilde{1}|3J_z^2 - J(J+1)|\tilde{1}\rangle, \qquad (19)$$

where taking the crystalline axis of the cube as the quantization axis $|\tilde{1}\rangle$ is expressed by

$$|\tilde{1}\rangle = \frac{1}{\sqrt{8}}(\sqrt{7}|J_z=3\rangle - |J_z=-1\rangle), \qquad (20)$$

and taking the threefold axis of the cube as the quantization axis

$$|\tilde{1}\rangle = \frac{1}{3\sqrt{6}}(|J_z=-2\rangle + 5|J_z=1\rangle - 2\sqrt{7}|J_z=4\rangle). \qquad (21)$$

Using the numerical value $\langle r_q^{-3}\rangle = 6.249$ a.u. with the relativistic corrections,[23,25] the EFG under the crystalline field is evaluated to be 8.289×10^{22} V/m^2 by taking the threefold axis of the cube as the axis of quantization, because magnetic moments should be parallel to $\langle 111\rangle$ in the $3\boldsymbol{k}$ structure as discussed in Sec. IV B. Then, assuming the Sternheimer factor as 0.35 ± 0.1, estimated for a $5f^1$ state,[29] we obtain the nuclear electric quadrupole interaction in the Γ_5 state induced by magnetic ordering:

$$\frac{e^2q_{5f}Q}{h}(1-R_{5f}) = 534\pm82\ \mathrm{MHz}, \qquad (22)$$

which is of the same order as the observed nuclear electric quadrupole interaction of 192 MHz for $\theta=0$ or 396 MHz for $\theta=\pi/2$ in Eq. (4). Here, $\theta=0$ is more likely because the symmetry axis should be determined by the direction of magnetic moments, considering the EFG induced by magnetic ordering. As a result, the EFG produced by the $5f$ electrons should be one of the major contributions at the ^{235}U sites. In addition, we should note that the second term in Eq. (17) can be also comparable with the first term by a large antishielding factor $\gamma_\infty \sim -100$ for heavy ions[30] although the eq_{lattice} is two orders of magnitude lower than eq_{5f}. Using $\gamma_\infty = -150$ for Am,[25] the second term $e^2q_{\mathrm{lattice}}Q(1-\gamma_\infty)/h$ is estimated to be a negative value, -250 MHz, from a point charge approximation for the $3\boldsymbol{k}$ distortions. Thus, the total EFG is evaluated as ~280 MHz, which agrees reasonably with the observed value. In summary, the observed EFG at the ^{235}U sites can be explained by a sum of the contributions from an axially symmetric $5f$ wave function and from the JT distortion which gives rise to an axially symmetric EFG. In the next section, we discuss the JT distortions in more detail on the basis of the ^{17}O NMR results because the EFG at the ^{17}O sites is dominated by only a contribution from the second term in Eq. (17).

B. Magnetic ordering and Jahn-Teller distortion

According to the neutron scattering experiments, the magnetic structure of UO_2 is a multi-$\boldsymbol{k}$ ($2\boldsymbol{k}$ or $3\boldsymbol{k}$) structure with a displacement of the oxygen atoms from their equilibrium position.[6,10–12] In this study, the JT distortion is clearly observed just below T_N through the appearance of the EFG at the ^{17}O sites, which should be mainly due to the lattice distortion term in Eq. (17). In this section, we discuss the magnetic structure and the JT distortion of UO_2 from the point of view of the ^{17}O NMR experiments. Our results are as follows:

(1) $H_{\rm int}=0.74\pm0.02$ T below 16 K,
(2) $\nu_Q=9.3\pm0.2$ kHz below 16 K,
(3) $H_{\rm int}//V_{ZZ}$,
(4) EFG tensor at the ^{17}O sites is axial ($\eta=0$),

where $\eta=(V_{YY}-V_{XX})/V_{ZZ}$ and (X,Y,Z) are the principal axes of the EFG tensor V at the ^{17}O sites. In Fig. 1, the $3\boldsymbol{k}$ structure has a threefold rotation axis at each oxygen site while the distortion in the $2\boldsymbol{k}$ structure is orthorhombic. Considering the symmetry of the lattice distortion, the observed axially symmetric EFG tensor indicates that the $3\boldsymbol{k}$ structure is realized. In order to verify the $3\boldsymbol{k}$ structure in more detail, we calculated the classical dipolar field and the EFG tensor due to lattice charges.

First, the classical dipolar field at the oxygen atoms is given by

$$\langle \boldsymbol{H}^{i}_{\rm dip}\rangle=\sum_j 3\frac{\langle\boldsymbol{\mu}_j\rangle\cdot\boldsymbol{r}_{ij}}{r_{ij}^5}-\frac{\langle\boldsymbol{\mu}_j\rangle}{r_{ij}^3}, \qquad (23)$$

where $\langle\boldsymbol{\mu}_j\rangle$ is the time average of the electronic spin moment at the jth atom at distance $\boldsymbol{r}_{ij}$ from the ith atom. The dipolar field is calculated by summation over 20 unit cells for each case of the $2\boldsymbol{k}$ and $3\boldsymbol{k}$ structure in Fig. 1. Here, we neglect the lattice distortion, because the small displacement of the oxygen atoms by 0.014 Å does not affect the magnitude and direction of the internal field. Using the ordered moment $1.74\mu_B$, dipolar fields at the oxygen sites are estimated to be about 0.42 T for both structures, which is comparable to the experimental value. The direction of $\langle\boldsymbol{H}^{i}_{\rm dip}\rangle$ is represented in Figs. 10(a) and 10(b). For the $2\boldsymbol{k}$ structure, $\langle\boldsymbol{H}^{i}_{\rm dip}\rangle$ points along the $\langle 101\rangle$ directions of the cubic unit cell, whereas for the $3\boldsymbol{k}$ structure it points along the $\langle 111\rangle$ directions.

Next, we have calculated the EFG tensor at the oxygen sites for the $2\boldsymbol{k}$ and the $3\boldsymbol{k}$ structures in a point charge approximation. For the oxygen ions with closed electron shells, the EFG should be mainly due to surrounding lattice charges. Since the oxygen sites have cubic local symmetry in the paramagnetic state, the observed EFG in the AFM state indicates the appearance of a lattice distortion. The EFG tensor V_{mn} produced by an ion of charge Ze at $\boldsymbol{r}$ can be written

$$V_{mn}=\frac{Ze(3r_mr_n-r^2\delta_{mn})}{r^5}, \qquad (24)$$

where we take m and n to represent the cubic axes. The EFG tensor is calculated from a summation over 20 unit cells. We determine the principal axis of the EFG tensor by diagonalizing the calculated one. When the principal component of the EFG tensor is defined as $|V_{ZZ}|\geqslant|V_{YY}|\geqslant|V_{XX}|$, we get for the (1/4,1/4,1/4) oxygen site with a displacement of 0.014 Å in the $2\boldsymbol{k}$ structure,

$$V_{XX}=-0.03\times10^{19}\ {\rm V/m^2},$$
$$V_{YY}=-2.75\times10^{19}\ {\rm V/m^2}, \qquad (25)$$
$$V_{ZZ}=2.78\times10^{19}\ {\rm V/m^2},$$

where $\mathbf{X}=(0,1,0)$, $\mathbf{Y}=(1/\sqrt{2})(1,0,-1)$, and $\mathbf{Z}=(1/\sqrt{2})(-1,0,-1)$. In the $3\boldsymbol{k}$ structure, we get

$$V_{XX}=-1.61\times10^{19}\ {\rm V/m^2},$$
$$V_{YY}=-1.61\times10^{19}\ {\rm V/m^2}, \qquad (26)$$
$$V_{ZZ}=3.21\times10^{19}\ {\rm V/m^2},$$

where $\mathbf{X}=(1/\sqrt{6})(-2,1,1)$, $\mathbf{Y}=(1/\sqrt{2})(0,1,-1)$, and $\mathbf{Z}=(1/\sqrt{3})(1,1,1)$. In these calculations we neglect the EFG produced by neighboring oxygen ions because it is $\sim10^{16}$ V/m^2. As seen in Fig. 11, the Z axes at the (1/4, 1/4,1/4) oxygen sites for the $2\boldsymbol{k}$ and $3\boldsymbol{k}$ structures are the

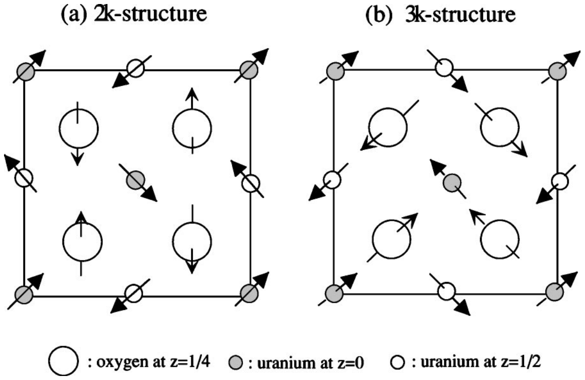

FIG. 10. The (001) projections of the fluorite structure for the $2\boldsymbol{k}$ and the $3\boldsymbol{k}$ structures. The dipolar fields at the oxygen atoms point along the $\langle 101\rangle$ directions for the $2\boldsymbol{k}$ structure and along the $\langle 111\rangle$ directions for the $3\boldsymbol{k}$ structure.

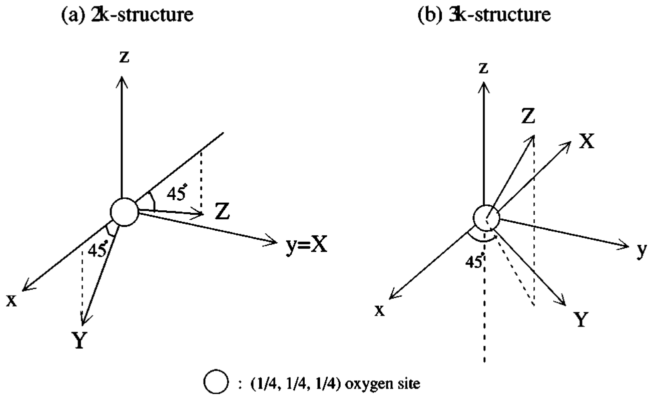

FIG. 11. The principal axis of the EFG tensor (the XYZ frame) at a (1/4, 1/4, 1/4) oxygen site. The (x,y,z) frame is taken for the cubic crystalline axis.

$(\bar{1}0\bar{1})$ and (111) directions, respectively. In the same way, we can calculate the EFG tensors for all eight oxygen sites equivalent to (1/4,1/4,1/4) and $(1/4,1/4,-1/4)$. The Z axes for these oxygen sites occupy all four $\langle 101\rangle$ directions for the $2\boldsymbol{k}$ structure and all eight $\langle 111\rangle$ directions for the $3\boldsymbol{k}$ structure. For the correct evaluation of the EFG tensor, one needs to consider the Sternheimer antishielding factor γ_∞ in Eq. (17).[27] The EFG tensor components can therefore be written $V_{ZZ}(1-\gamma_\infty)$. In this analysis, however, we ignore the antishielding effect, because it does not affect the determination of the principal axis of the EFG tensor. Then, the quadrupole frequency and the asymmetry parameter for the $2\boldsymbol{k}$ structure are evaluated to be

$$\begin{aligned}\nu_Q&=2.6\ \text{kHz}\quad (Z\|H_{\text{dip}}),\\ \eta&\simeq 1,\end{aligned}\tag{27}$$

and for the $3\boldsymbol{k}$ structure,

$$\begin{aligned}\nu_Q&=3.0\ \text{kHz}\quad (Z\|H_{\text{dip}}),\\ \eta&=0,\end{aligned}\tag{28}$$

where we use $-2.6\times10^{-30}\ \text{m}^2$ as the nuclear quadrupole moment of the ^{17}O nucleus. In both cases of multi-$\boldsymbol{k}$ structures, the amplitude of the calculated EFG is comparable to the experimental value [result (2)], and the experimental result (3) is also fulfilled. From the asymmetry parameter in result (4), however, the $2\boldsymbol{k}$ structure is excluded and the $3\boldsymbol{k}$ structure is the more likely of the proposed multi-$\boldsymbol{k}$ structures.

C. Low-energy excitations

Interacting with nuclear spins as a result of hyperfine coupling, spin waves (or magnons) can be scattered by nuclear spins, as well as absorbed and emitted by them; finally, spin waves can be converted into lattice vibrations (phonons). Thus the relaxation process caused by fluctuating local fields at the nucleus gives us important knowledge on spin-wave excitations. Direct processes, in which the nuclear spin is flipped and a spin wave is absorbed or emitted, are usually unimportant because of energy conservation. However, Raman processes, in which the nuclear spin flip arises from the absorption of a spin wave of energy $\hbar\omega_k$ and the simultaneous emission of another spin wave of energy $\hbar\omega_{k'}$, as $|\hbar\omega_k-\hbar\omega_{k'}|$ is equal to the nuclear Zeeman energy, can be a major contribution in the relaxation process. The T dependence of T_1^{-1} due to two-magnon Raman processes is expressed in the small-$\boldsymbol{k}$ approximation by $T_1^{-1}\propto T^3$ and $T^2\exp(-T_{\text{AE}}/T)$ for $T\gg T_{AE}$ and $T\ll T_{\text{AE}}$, respectively,[31] where $k_{\text{B}}T_{\text{AE}}$ is the initial gap in the spin-wave spectrum. For $T\ll T_{\text{AE}}$, the gap has a pronounced effect. This character at $T\ll T_{\text{AE}}$ is also expected for processes with the participation of three or more magnons. In UO$_2$, however, the T dependence of T_1^{-1} between 4.2 and 25 K shows a T^7 behavior over six orders of the magnitude as seen in Fig. 3. Since the energy gap is estimated as about 28 K from the spin-wave spectrum,[7] this T^7 behavior is in the region of $T<T_{\text{AE}}$. Here, we notice that a quasiphonon branch observed by Cowley and Dolling[7] has no gap in the dispersion, $E\sim|\mathbf{k}|$. In general, relaxation processes due to phonon excitations are dominant only for quadrupole relaxation which arises from the interaction between the nuclear quadrupole moments and fluctuations in the EFG. In the case of UO$_2$, the quadrupole relaxation due to pure phonon excitations is unlikely, because recovery curves at the ^{235}U sites can be fit by a multiexponential function characteristic of magnetic relaxation processes [Eq. (3)]. It is known that coupling between spin-wave and phonon modes mixes spin-wave character into the phonons and thereby allows the phonons to induce magnetic processes directly. This quasiphonon branch might be particularly important for the magnetic relaxation process at $T\ll T_{\text{AE}}$. The relaxation rate due to Raman processes of the mixed magnon-phonon modes is theoretically given as $T_1^{-1}\propto T^7$ for $T\ll T_{\text{AE}}$,[32] which agrees with the experimental result. This would be closely related with the strong spin-lattice interaction which causes the first-order phase transition of UO$_2$.

V. CONCLUSION

In order to investigate the exotic properties of quadrupolar ordering, we need experimental techniques to probe f quadrupoles (or f wave functions) directly as well as lattice distortions. Direct observation of ^{235}U NMR is a powerful technique to determine the local symmetry of $5f$ wave functions. In the long history of NMR studies, however, ^{235}U NMR had never been observed in solids. As a first step, we succeeded in observing ^{235}U NMR in UO$_2$. Important factors for this observation were the presence of a large hyperfine field and a long relaxation time in the AFM state, and use of a 93% ^{235}U-enriched sample. This means that we can observe ^{235}U NMR by selecting an appropriate material and using samples enriched with ^{235}U, although the nuclear magnetic moment is very small and the relaxation time will in many instances be too short.

We have measured the magnetic hyperfine interaction and the nuclear electric quadrupole interaction produced by $5f$ electrons, and confirmed that these can be successfully estimated from the numerical value of $\langle r^{-3}\rangle$ for a free U^{4+} ion. Like for $4f$ series, the main contribution to the magnetic hyperfine field arises from the orbital magnetic moment. However, since the calculated orbital hyperfine field for a free U^{4+} ion is comparable with that for a free U^{3+} ion, it will be difficult to distinguish the valence of a uranium ion from magnetic hyperfine measurements. Alternatively, the nuclear electric quadrupole interaction is expected to be very sensitive to the interaction of orbitals with the crystalline field. In the magnetic ordered state of UO$_2$ we observed an axially symmetric EFG, which indicates the presence of the uniaxial $5f$ wave function induced by magnetic ordering as well as the lattice distortions.

Below the transition temperature of UO$_2$, we observed oscillatory ^{17}O spin-echo modulation owing to the presence of an axially symmetric EFG at the oxygen sites and an internal field parallel to the symmetry axis. By analyzing the symmetry of possible lattice distortions, we have concluded that the 3***k*** structure is the most likely of the magnetic structures proposed by the neutron scattering experiments. This application of spin-echo modulation effect can be useful for NMR studies of a JT distortion in magnetic ordered states. The appearance of lattice distortion just below the AFM transition temperature is also clearly observed by this method. In addition, the T^7 dependence of T_1^{-1} in the AFM state for both ^{17}O and ^{235}U suggests the presence of a quasiphonon branch of $5f$ magnons due to strong magnon-phonon coupling, as measured by Cowley and Dolling.[7]

Finally, we note that this study shows the advantages of NMR experiments, that is, that microscopic properties can be selectively discussed for each site in a given compound. In ^{235}U NMR experiments we have directly detected local information with respect to the $5f$ wave functions, and in ^{17}O NMR experiments we have obtained spatial information about the magnetic structure and the JT distortion through the internal field and the EFG produced by surrounding U^{4+} and O^{2-} ions.

ACKNOWLEDGMENTS

We wish to thank Professor G. H. Lander for helpful discussions about magnetic properties of UO_2. In addition, we wish to thank Dr. M. Date and Dr. M. Saeki for providing ^{235}U-enriched uranium samples at the Japan Atomic Energy Research Institute. S.N. and Y.O. were financially supported by a Grant-in-Aid for COE Research (No. 10CE 2004) from the Ministry of Education, Science, Sports and Culture.

---

[1] K.A. McEwen, U. Steigenberger, and J.L. Martinez, Physica B **186-188**, 670 (1993).

[2] P. Santini, G. Amoretti, R. Caciuffo, F. Bourdarot, and B. Fak, Phys. Rev. Lett. **85**, 654 (2000).

[3] H.U. Rahman and W.A. Runciman, J. Phys. Chem. Solids **27**, 1833 (1966); **30**, 2497 (1969); H.U. Rahman, Physica (Amsterdam) **45**, 511 (1970).

[4] S. Kern, C.K. Loong, and G.H. Lander, Phys. Rev. B **32**, 3051 (1985); G. Amoretti, A. Blaise, R. Caciuffo, J.M. Fournier, M.T. Hutchings, R. Osborn, and A.D. Taylor, *ibid.* **40**, 1856 (1989).

[5] B.C. Frazer, G. Shirane, D.E. Cox, and C.E. Olsen, Phys. Rev. **140**, A1448 (1965).

[6] J. Faber, Jr. and G.H. Lander, Phys. Rev. B **14**, 1151 (1976).

[7] R.A. Cowley and G. Dolling, Phys. Rev. **167**, 464 (1968).

[8] S.J. Allen, Phys. Rev. **166**, 530 (1968); **167**, 492 (1968).

[9] R. Caciuffo, G. Amoretti, P. Santini, G.H. Lander, J. Kulda, and P. de V. Du Plessis, Phys. Rev. B **59**, 13 892 (1999).

[10] J. Rossat-Mignod, G.H. Lander, and P. Burlet, in *Handbook on the Physics and Chemistry of the Actinides*, edited by A. J. Freeman and G. H. Lander (North-Holland, Amsterdam, 1984), p. 415.

[11] I.E. Dzyaloshinskii, Commun. Phys. **2**, 69 (1977).

[12] P. Burlet, J. Rossat-Mignod, S. Quezel, O. Vogt, J.C. Spirlet, and J. Rebizant, J. Less-Common Met. **121**, 121 (1986).

[13] K. Ikushima, Y. Kato, M. Takigawa, F. Iga, S. Hiura, and T. Takabatake, Physica B **281&282**, 274 (2000).

[14] K. Ikushima, H. Yasuoka, S. Tsutsui, M. Saeki, S. Nasu, and M. Date, J. Phys. Soc. Jpn. **67**, 65 (1998).

[15] K. Ikushima, H. Yasuoka, S. Tsutsui, S. Nasu, N.M. Masaki, A. Nakamura, and Y. Ueda, Physica B **281&282**, 197 (2000).

[16] S.L. Ruby, G.M. Kalvius, B.D. Dunlap, G.K. Shenoy, D. Cohen, M.B. Brodsky, and D.J. Lam, Phys. Rev. **184**, 374 (1969).

[17] S. Tsutsui, M. Nakata, N.M. Masaki, M. Saeki, S. Nasu, A. Nakamura, Y. Haga, E. Yamamoto, and Y. Onuki, Hyperfine Interact. C **3**, 225 (1998).

[18] T. Moriya, Prog. Theor. Phys. **16**, 641 (1956).

[19] W.J.L. Buyers and T.M. Holden, in *Handbook of the Physics and Chemistry of the Actinides*, edited by A.J. Freeman and G.H. Lander (North-Holland, Amsterdam, 1985), Vol. 2, p. 239.

[20] H. Abe, H. Yasuoka, and A. Hirai, J. Phys. Soc. Jpn. **21**, 77 (1966).

[21] A. Abragam, *Principles of Nuclear Magnetism* (Clarendon, Oxford, 1961), p. 258.

[22] See, e.g., A. Abragam and B. Bleaney, *Electron Paramagnetic Resonance of Transition Ions* (Oxford University Press, New York, 1970), p. 680.

[23] W.B. Lewis, J.B. Mann, D.A. Liberman, and D.T. Cromer, J. Chem. Phys. **53**, 809 (1970).

[24] C.J. Lenander, Phys. Rev. **130**, 1033 (1963).

[25] B.D. Dunlap and G.M. Kalvius, in *The Actinides: Electronic Structure and Related Properties*, edited by A. J. Freeman and J. B. Darby, Jr. (Academic Press, New York, 1974), p. 237.

[26] N. Edelstein and R. Mehlhorn, Phys. Rev. B **2**, 1225 (1970).

[27] R.M. Sternheimer, Phys. Rev. **84**, 244 (1951).

[28] R.J. Elliott and K.W.H. Stevens, Proc. R. Soc. London, Ser. A **218**, 553 (1953).

[29] B.D. Dunlap, G.M. Kalvius, and G.K. Shenoy, Phys. Rev. Lett. **26**, 1085 (1971).

[30] R.M. Sternheimer, Phys. Rev. **146**, 140 (1966).

[31] V. Jaccarino, in *Magnetism II*, edited by G.T. Rado and H. Suhl (Academic Press, New York, 1966), p. 307.

[32] P. Pincus and J. Winter, Phys. Rev. Lett. **7**, 269 (1961).